HHS Public Access

Author manuscript

Biotechnol Bioeng. Author manuscript; available in PMC 2019 January 01.

Published in final edited form as:

Biotechnol Bioeng. 2018 January ; 115(1): 232–245. doi:10.1002/bit.26442.

Glucose-Stimulated Insulin Release: Parallel Perifusion Studies of Free and Hydrogel Encapsulated Human Pancreatic Islets

Peter Buchwald[1,2,*], **Alejandro Tamayo-Garcia**[1], **Vita Manzoli**[1,3], **Alice A. Tomei**[1,4], and **Cherie L. Stabler**[5]

[1]Diabetes Research Institute, University of Miami, Miller School of Medicine, Miami, FL

[2]Department of Molecular and Cellular Pharmacology, University of Miami, Miller School of Medicine, Miami, FL

[3]Department of Electronics, Information and Bioengineering, Politecnico di Milano, Italy

[4]Biomedical Engineering, University of Miami, Miller School of Medicine, Miami, FL

[5]Department of Biomedical Engineering, University of Florida, Gainesville, FL, USA

Abstract

To explore the effects immune-isolating encapsulation has on the insulin secretion of pancreatic islets and to improve our ability to quantitatively describe the glucose-stimulated insulin release (GSIR) of pancreatic islets, we conducted dynamic perifusion experiments with isolated human islets. Free (unencapsulated) and hydrogel encapsulated islets were perifused, in parallel, using an automated multi-channel system that allows sample collection with high temporal resolution. Results indicated that free human islets secrete less insulin per unit mass or islet equivalent (IEQ) than murine islets and with a less pronounced first-phase peak. While small microcapsules ($d \approx$ 700 μm) caused only a slightly delayed and blunted first-phase insulin response compared to unencapsulated islets, larger capsules ($d \approx$ 1800 μm) completely blunted the first-phase peak and decreased the total amount of insulin released. Experimentally obtained insulin time-profiles were fitted with our complex insulin secretion computational model. This allowed further fine-tuning of the hormone-release parameters of this model, which was implemented in COMSOL Multiphysics to couple hormone secretion and nutrient consumption kinetics with diffusive and convective transport. The results of these GSIR experiments, which were also supported by computational modeling, indicate that larger capsules unavoidably lead to dampening of the first-phase insulin response and to a sustained-release type insulin secretion that can only slowly respond to changes in glucose concentration. Bioartificial pancreas type devices can provide long-term and physiologically desirable solutions only if immunoisolation and biocompatibility considerations are integrated with optimized nutrient diffusion and insulin release characteristics by design.

[*]Corresponding author. University of Miami, DRI, 1450 NW 10th Ave (R-134), Miami, FL 33136, USA, pbuchwald@med.miami.edu, Tel.: (1) 305 243-9657.

Competing interests

The author(s) declare that they have no competing interests.

Authors' contributions

PB conceived the study, analyzed the data, performed the computational modeling, and drafted the manuscript; ATG performed the islet isolation and perifusion experiments; VM and AAT carried out the islet encapsulations; AAT and CLS participated in the design of the study and in the writing of the manuscript. All authors read and approved the final manuscript.

Keywords

alginate; diabetes mellitus; islet encapsulation; FEM model; fluid dynamics; glucose-stimulated insulin secretion

Introduction

Patients with type 1 diabetes (T1D) lose their ability to produce insulin and require lifelong administration of exogenous insulin. Technological improvements, such as continuous glucose monitoring systems and continuous subcutaneous insulin infusion (Thabit *et al.*, 2016) have provided improvements, but they are still not successful in all patients. Because such therapies cannot fully reproduce the inherently complex function of the endocrine pancreas, chronic and degenerative complications are still unavoidable in long-term T1D. With improved management and control, some complications have declined (Pambianco *et al.*, 2006; Gregg *et al.*, 2014), but others have not, especially in long-term patients (>30 years) (Pambianco *et al.*, 2006). Transplantation of pancreatic islet cells can provide insulin independence with proven safety and efficacy, and it is likely to become an approved clinical treatment in T1D patients complicated by severe hypoglycemia (Ricordi *et al.*, 2004; Fiorina *et al.*, 2008; Hering *et al.*, 2016; Shapiro *et al.*, 2017). Furthermore, stem cell therapies are becoming increasingly likely to provide novel cell sources (Johnson, 2016; Mahla, 2016) that overcome the problem of limited donors, considerably widening the applicability of such approaches. Nevertheless, to prevent allograft rejection, cellular transplantations require the use of systemic immunosuppression, which imposes a considerable burden on the patient and limits widespread applicability. As a possible approach to circumvent immunorecognition and rejection, islet (micro)encapsulation has been extensively explored since the 1980s (Soon-Shiong, 1999; Silva *et al.*, 2006; Teramura *et al.*, 2010; O'Sullivan *et al.*, 2011; Calafiore *et al.*, 2014; Colton, 2014; Scharp *et al.*, 2014; Steele *et al.*, 2014; Desai *et al.*, 2016; Song *et al.*, 2016). The failure of several clinical and preclinical attempts made it clear that these approaches also have challenges and long-term functionality is not easily achieved (King, 2009; Scharp *et al.*, 2014).

To explore how encapsulation affects insulin secretion and to improve our ability to quantitatively describe the glucose-stimulated insulin release (GSIR) of pancreatic islets, here, we performed dynamic perifusion experiments with free (unencapsulated) and immunoisolated human islets using an automated multi-channel apparatus that allows parallel for perifusion and sample collection with high temporal resolution. Such dynamic GSIR perifusion studies (Figure 1) have been introduced in the early 1970s (Lacy *et al.*, 1972). With improved equipment and analytical techniques, they now allow good quantitative characterization of insulin release kinetics under fully controllable experimental conditions of varying external concentrations of glucose and secretagogues of interest (Dionne *et al.*, 1993; Sweet *et al.*, 2002; Bocca *et al.*, 2008; Cabrera *et al.*, 2008; Buchwald *et al.*, 2015; Garcia-Contreras *et al.*, 2017). Perifusion studies are also emerging as a useful assay of islet quality and function for research and clinical applications (Kayton *et al.*, 2015). Here, we investigated the insulin release kinetics of alginate encapsulated islets (small and large capsules) comparing them to those of free islets perifused in parallel. The

corresponding experimentally obtained data also allowed us to perform more detailed theoretical investigations using our recently developed complex computational model of insulin secretion (Buchwald, 2011; Buchwald *et al.*, 2013; Buchwald *et al.*, 2015).

Materials and Methods

Islet isolation and encapsulation

Human islet samples were procured from isolations performed at the Human Islet Cell Processing Facility at the Diabetes Research Institute (University of Miami, Miller School of Medicine, Miami, FL, USA). The islet isolation protocol, as part of the Clinical Pancreatic Islet Transplantation Study, was approved by the institutional review board (IRB) of the University of Miami and the FDA. Human pancreases were isolated from deceased multi-organ donors for whom consent for transplantation was obtained by accredited organ procurement organizations (OPO) from the donor's families or next of kin. Islets were isolated by using a modification of the automated method (Ricordi *et al.*, 1988) as described previously (Khan *et al.*, 2009; Ricordi *et al.*, 2016). Mouse islets used for some additional perifusion experiments were obtained and processed as described before (Buchwald *et al.*, 2015). All animal studies were reviewed and approved by the University of Miami Institutional Animal Care and Use Committee. All procedures were conducted according to the guidelines of the Committee on Care and Use of Laboratory Animals, Institute of Laboratory Animal Resources (National Research Council, Washington DC). Animals were housed in microisolated cages in Virus Antibody Free rooms with free access to autoclaved food and water at the Department of Veterinary Resources of the University of Miami. Islets were obtained from donor mice (BALB/C or C57BL6/J, Jackson Lab, Bar Harbor, ME) via mechanically enhanced enzymatic digestion followed by density gradient purification using a procedure similar to that previously described (Pileggi *et al.*, 2001; Rengifo *et al.*, 2014). Briefly, animals were sacrificed under general anesthesia, and the pancreas was exposed and injected with Hanks' balanced salt solution (HBSS; Mediatech, Herndon, VA) containing either 0.8 mg/mL collagenase type V (Sigma-Aldrich, St. Louis, MO) or a mix of 0.2 mg/mL Liberase TL and 0.1 mg/mL DNase (Roche, Indianapolis, IN) via the main bile duct until distension was achieved. Digestion was performed at 37°C for 10–15 min with gentle shaking and terminated by the addition of cold RPMI–10% fetal bovine serum (FBS) with 20×10^{-3} M Hepes buffer, 1% penicillin-streptomycin, and 1% L-glutamine (all from Sigma-Aldrich). Mechanical disruption of the pancreas was achieved by passages through needles of decreasing gauge until release of islets was observed under a microscope; the tissue was filtered through a 450 μm mesh, and islets were purified on Euro-Ficoll (Mediatech) gradients by centrifugation at 400 g for 15–20 min, routinely yielding preparations of 90% purity.

Islet purity was assessed by dithizone (Sigma-Aldrich) staining, and islets were counted and scored using a standard algorithm for the calculation of 150 μm diameter islet equivalent (IEQ) number (Ricordi *et al.*, 1990; Buchwald *et al.*, 2009). Murine islets were cultured in complete CMRL 1066-based medium, which is CMRL 1066 (Mediatech; contains 1 g/L = 5.56 mM glucose) with 10% fetal bovine serum (FBS), 20 mM HEPES buffer, 1% penicillin-streptomycin, and 2 mM L-glutamine added (all from Sigma-Aldrich). Human

islets were cultured in CMRL-1066 supplemented medium (Mediatech; contains 5.56 mM glucose, 25 mM HEPES, 1 g/L = 4.6 mM L-alanine–L-glutamine) with 2% human serum albumin (HSA) added, at 37°C in 5% CO_2 humidified incubator for 24 h prior to encapsulation, and perifusions were performed 24–48 h after encapsulations. For encapsulation, standard Ca-alginate microbeads were fabricated using a modification of the protocol originally developed by Lim and Sun (Lim *et al.*, 1980). Briefly, 1.2% (w/v) alginate (UP-MVG, MW 300 kDa, MW/Mn= 1.87, DPn of 28, Batch # FP-504-03, Pronova Novamatrix, FMC) dissolved in HBSS was homogeneously mixed with pelleted islets prior to extrusion through a electrostatic droplet generator (Nisco Engineering, Zurich, Switzerland) into a crosslinking bath of 50 mM calcium chloride, supplemented with 10 mM 3-(N-morpholino)propanesulfonic acid (MOPS), 140 mM D-Mannitol, and 0.025% Tween-20. After crosslinking (10 min), microbeads were washed with HBBS and cultured for 24–48 h prior to study. Resulting beads had average sizes of 700 μm (small capsules) and 1800 μm (large capsules). Small capsules contained an average of 2.9 ± 1.7 islets (corresponding to 4.7 ± 3.9 IEQs), whereas large capsules contained an average of 8.8 ± 2.8 islets (corresponding to 11.4 ± 5.7 IEQs).

Islet perifusion

The perifusion experiments (dynamic GSIR) were performed using a PERI4-02 machine (Biorep Technologies, Miami, FL, USA) that allows parallel perifusion for up to eight independent channels. For each experiment, one hundred free (unencapsulated) or encapsulated islets (all from the same isolation batch) were handpicked and loaded in Perspex microcolumns between two layers of acrylamide-based microbead slurry (Bio-Gel P-4, Bio-Rad Laboratories, Hercules, CA) by the same experienced operator. Perifusing buffer containing 125 mM NaCl, 5.9 mM KCl, 1.28 mM $CaCl_2$, 1.2 mM $MgCl_2$, 25 mM HEPES, and 0.1% bovine serum albumin at 37°C with selected glucose (low = 3 mM; high = 11 mM) or KCl (25 mM) concentrations was circulated through the columns at a rate of 100 μL/min. After 45–60 minutes of washing with the low glucose solution for stabilization, islets were stimulated with the following sequence: 5 min of low glucose, 20 min of high glucose, 15 min of low glucose, 10 min of KCl, and 10 min of low glucose. Serial samples (100 μL) were collected every minute from the outflow tubing of the columns in an automatic fraction collector designed for a multi-well plate format. The sample container harboring the islets and the perifusion solutions were kept at 37°C in a built-in temperature controlled chamber. The perifusate in the collecting plate was kept at <4°C to preserve the integrity of the analytes. Insulin concentrations were determined with commercially available ELISA kits (Mercodia Inc., Winston Salem, NC). Values obtained with the human kit are in mU/L; they were converted to μg/L using 1 μg/L = 23 mU/L per the guidelines of the manufacturer. Evaluation of islet mass (IEQ) is challenging and error-prone (Buchwald *et al.*, 2016), and it is especially so for encapsulated islets. Therefore, as before (Buchwald *et al.*, 2015), to account for possible differences in islet mass (IEQ) among islets in different channels, values were rescaled by a normalization factor so as to make the area under the curve (AUC) for the KCl-induced release of insulin in each channel similar to that of the free islets used as a reference. Data used here are averages of at least three samples for each condition.

Computational methods

For computational modeling, our previously developed local concentration-based insulin secretion model has been used. A conceptual schematic of the model is shown in Figure 2; detailed descriptions of its implementation and parameterization have been published (Buchwald, 2011; Buchwald *et al.*, 2015). Briefly, a total of four concentrations are used for (convective and diffusive) mass transport modeling, with their corresponding equations (application modes): glucose, oxygen, and 'local' and released insulin (c_{gluc}, c_{oxy}, c_{insL}, c_{ins}). Diffusion is assumed to be governed by the generic diffusion equation in its nonconservative formulation (incompressible fluid):

$$\frac{\partial c}{\partial t}+\nabla\cdot(-D\nabla c)=R-\boldsymbol{u}\cdot\nabla c \quad (1)$$

where c denotes the concentration [mol·m^{-3}], D the diffusion coefficient [m^2·s^{-1}], R the reaction rate [mol·m^{-3}·s^{-1}], **u** the velocity field [m·s^{-1}], and ∇ the standard *del* (*nabla*) operator ($\nabla\equiv\boldsymbol{i}\frac{\partial}{\partial x}+\boldsymbol{j}\frac{\partial}{\partial y}+\boldsymbol{k}\frac{\partial}{\partial z}$). Diffusion coefficients (D) used are from the original model (Buchwald, 2011); they were selected as consensus estimates of values available from the literature, and are summarized in Table 1. All consumption and release rates are assumed to follow Hill–type dependence (generalized Michaelis-Menten kinetics) on the local concentrations as this provides a convenient and easily parameterizable mathematical function:

$$R=f_H(c)=R_{max}\frac{c^n}{c^n+c^n_{Hf}} \quad (2)$$

In all cases (i.e., insulin, glucose, oxygen), R_{max} denotes the maximum reaction rate [mol·m^{-3}–s^{-1}], C_{Hf}, the concentration corresponding to half-maximal response [mol·m^{-3}], and n, the Hill slope characterizing the shape of the response. The parameter values used are summarized in Table 2; they are generally the same as in the original model (Buchwald, 2011), except for those explicitly discussed in the Results. Total insulin release is obtained as the sum of the first- and second-phase releases (plus an additional modulating function to account for the limiting effect of oxygen availability):

$$R_{ins}=(R_{ins,ph1}+R_{ins,ph2})\cdot\varphi_{i,o}(c_{oxy}) \quad (3)$$

For human islets, these two R_{ins} values were now slightly rescaled (decreased, see Table 2) to better fit the experimental data, as well as recent detailed dose-response GSIR experimental data from Henquin and co-workers (Henquin *et al.*, 2015). For a correct time-scale of insulin release, an additional 'local' insulin compartment is included in the model (Figure 1) so that insulin is assumed to be first secreted into this compartment and then released following first order kinetics, $\frac{dc_{insL}}{dt}=R_{ins}-k_{insL}(c_{insL}-c_{ins})$ (Buchwald, 2011). The original model, which was calibrated for human islets, used a corresponding rate constant of k_{insL} = 0.003 s^{-1}; for murine islets, this was modified to have a slightly faster release to 0.006 s^{-1} (Buchwald *et al.*, 2015). Finally, to incorporate media flow, these convection and

diffusion models are coupled to a fluid dynamics model. The flowing media is assumed to be an aqueous media at physiological temperature (37°C). Incoming media is assumed to be in equilibrium with atmospheric oxygen and, thus, to have an oxygen concentration of $c_{oxy,in}$ = 0.200 mol·m^{-3} (mM) corresponding to $p_{O_2} \approx 140$ mmHg. For physiologically relevant conditions, lower values have to be used as tissue oxygen concentrations are likely to be around only $c_{oxy,tis}$ = 0.060 mol·m^{-3} (mM) (corresponding to $p_{O_2} \approx 40$ mmHg (5%)), as the average oxygen concentrations in arterial and venous blood are ~0.130 and ~0.054 mM (corresponding to ~12% and ~5%, respectively) (Fournier, 2011).

The model is implemented in COMSOL Multiphysics (COMSOL Inc., Burlington, MA) and solved as a time-dependent (transient) problem, allowing intermediate time-steps for the solver, as described previously. Mesh and boundary conditions used are as described before (Buchwald, 2011; Buchwald *et al.*, 2015). Similar to our previous models (Buchwald, 2011; Buchwald *et al.*, 2013; Buchwald *et al.*, 2015), here, we also used two spherical islets of 100 and 150 μm diameter placed in a 2D cross-section of a cylindrical tube with fluid flowing from left to right (see Figure 7 for an illustration of the geometry used). Islet sizes were selected based on our analyses of the size distribution of isolated islets (Buchwald *et al.*, 2009; Buchwald *et al.*, 2016), which found that for isolated human islets, the expected value of diameter is 95 μm while the expected value of volume corresponds to that of an islet with diameter of 133 μm. Islets are considered homogeneous inside; individual cells (e.g., α- or β-cells) are not considered separately.

Results

Dynamic perifusions of isolated (avascular) islets were performed using a low (3 mM, G3) → high (11 mM, G11) → low (3 mM, G3) glucose step followed by a KCl step in a fully automated machine that allows parallel perifusion in up to eight channels and frequent sample collection (every minute). As before (Buchwald *et al.*, 2015; Garcia-Contreras *et al.*, 2017), the high glucose step (G11) was maintained for 20 min to allow a clear delineation of the first-phase response.

Human versus murine islets

Average insulin responses obtained from perifusion of several islet samples are shown in Figure 3 to compare the insulin secretion of free human and murine islets. Such unencapsulated islets typically show a well-defined first-phase peak, followed by a second-phase plateau as expected from normal functioning islets that are known to release insulin in a biphasic manner in response to a stepwise increase of glucose: a first phase of a relatively quick transient spike is followed by a sustained, but somewhat smaller second phase (Hedeskov, 1980; Henquin, 2000; Rorsman *et al.*, 2000; Henquin, 2009). Our results obtained here with the same perifusion protocol indicate that human islets secrete less insulin per islet equivalent (IEQ) than murine islets and with a less pronounced first phase peak. Comparison of the corresponding average secreted values (Figure 3) indicates an approximate three-fold difference during the peak of the 5–10 min first-phase (24.3 vs. 8.5 pg/IEQ/min) and an approximate two-fold difference during the following second-phase plateau (13.0 vs. 5.8 pg/IEQ/min).

Effect of small and large capsules

To directly evaluate the effects of hydrogel encapsulation on the insulin release profile of islets, we performed parallel dynamic GSIR perifusion assays with free and alginate encapsulated islets sourced from the same donor (Figure 4). Parallel channels were used for free islets, and the small ($d \approx 700$ μm) and large capsules ($d \approx 1800$ μm). Whereas the small capsules caused only a slightly delayed and blunted first-phase insulin response compared to free islets, the larger capsules completely blunted this first-phase peak. The same effect could also be seen in the response to the KCl step (Figure 4); clearly indicating a diffusion limitation problem. For the small capsules, the first-phase peak was delayed by about one minute and decreased by ~5% (6.9 vs. 7.2 pg/IEQ/min). With the large capsules, the delay was more than three minutes and the decrease is >40% (4.0 vs. 7.2 pg/IEQ/min). The second-phase plateau decreased somewhat for the small capsules (~30%; 3.6 vs. 5.2 pg/IEQ/min) and a bit less for the large capsules, as the tail of the first-phase peak overlaps due to the diffusional delay (~15%; 4.4 vs. 5.2 pg/IEQ/min).

Fit with computational model

A further goal of the present work was to fine-tune and improve the parametrization of our FEM-based COMSOL Multiphysics model of insulin secretion for avascular islets (Buchwald, 2011) and use it for the computational analysis of these results. The model assumes that the insulin-secreting β-cells act as sensors of both the local glucose concentration, c_{gluc}, and its change (i.e., its time-gradient), $\partial c_{gluc}/\partial t$, so that the first-phase response is related to how quickly the (local) glucose concentration changes and the second-phase response is related to the value of the (local) glucose concentration (Figure 2) (Buchwald, 2011). The original model (Buchwald, 2011) was parametrized for human islets and later modified slightly to describe murine islets (Buchwald *et al.*, 2015). To account for the somewhat sharper first-phase response of murine islets, a single parameter was changed (k_{insL} increased to 0.006 s^{-1} from the original 0.003 s^{-1}). Since we have now also obtained directly comparable insulin secretion rates in human versus murine islets (Figure 3), and they indicate a lower secretion per unit mass (IEQ) in human islets, the corresponding insulin secretion rates in human islets were recalibrated, as shown in Table 2. The effect of these changes on the predicted insulin secretion can be seen by comparing the calculated profiles for human and murine islets (dashed lines) in Figure 3. To further fine-tune the parameters of the present model, we have also fitted a set of additional GSIR data from three different dose-response experiments, published by Henquin and co-workers (Henquin *et al.*, 2006a; Henquin *et al.*, 2015) (Figure 5). To improve the fit, one additional change was required: the Hill slope of the modulating function for the first-phase response, $\sigma_{i1,g}$, was decreased from 4 to 2.5 to allow a first-phase peak over a wider range of glucose step-up. With these adjustments, the model can fit quite well the overall GSIR profile of human and mouse islets in our standard perifusion experiments (Figure 3), as well as the wider range of different profiles obtained for various incoming glucose step-up challenges (Figure 5). While most first-phase responses are fit well by the model; those for the G3 → G15 and G3 → G30 steps (Figure 5B) are under-predicted, likely because for these large steps, the glucose increase too rapidly making the gradient too large compared to the C_{Hf} parameter of the first-phase response $R_{ins,ph1}$ (0.03 mM/s, Table 2) and the glucose range moves too quickly out of the optimal range of the modulating function $\sigma_{i1,g}$.

The model was then applied to fit the insulin secretion profile of the hydrogel-encapsulated islets (Figure 6). Previously, we have already shown that because of increasing diffusional distances, the predicted insulin release profiles of encapsulates islets have an increasingly delayed and blunted response as capsule thickness increases (Buchwald, 2011; Buchwald *et al.*, 2015). This is in general agreement with the present experimental results. As before, all calculations shown here were performed with two representative islets with diameters of d = 100 and 150 μm. Predicted responses for the encapsulated islets agree well with the experimental GSIR time-profiles (Figure 6). The fits shown here were obtained with capsule thicknesses of l_{caps} = 100 μm for the small and l_{caps} = 400 μm for the large capsules as they gave the best fit (lowest sum of squared errors, SSE) in calculations with a parameter sweep for capsule thickness, l_{caps}, ranging from 50 to 500 μm in steps of 50. For a 'standard' single islet of 150 μm diameter (IEQ), these values correspond to capsules of 350 and 950 μm diameter – somewhat smaller than the alginate beads actually used ($d \approx$ 700 and 1800 μm). However, in reality, islets are not centrally located in fully symmetric capsules (see illustrative examples in Figure 4), and exchange with the bead surface can take place along shorter diffusional pathways, resulting in a smaller apparent diffusional distance. This accounts for the smaller apparent capsule size that provides the best fit in the computational model. In fact, for the large capsule, the fit could be further improved by placing the islets off-center, and the results shown here were obtained with islets placed 300 μm off-center.

The computational model allowed for detailed calculations of the spatial distribution (concentrations) of all species of interest and their changes, depending on the input conditions. For example, Figure 7 shows calculated insulin production rates for small and large alginate capsules during an increase in the incoming glucose concentration (i.e., during the first-phase response). Figure 8 presents model-calculated oxygen and glucose concentrations during high glucose (G11) exposure under normoxic conditions (atmospheric oxygen). These data are included to show that, in avascular islets, diffusion limitations are more severe for oxygen than for glucose. Thus, oxygen availability is the main issue limiting the functionality and viability of such islets (see Discussion for further details).

Discussion

Human versus murine islets

According to our dynamic GSIR perifusion experiments, human islets, on average, secrete approximately two- to three-fold less insulin per unit mass (IEQ) than murine islets and with a less pronounced first phase peak (Figure 3). This is even more remarkable when accounting for the fact that the high glucose level used in this study (11 mM) likely provides a stronger stimulus for human than mouse islets, as human islets initiate insulin secretion at lower glucose levels than mouse islets and are likely to have a lower $C_{Hf,ins}$ (Henquin *et al.*, 2006a; Henquin *et al.*, 2006b; Henquin *et al.*, 2015). Note, however, that there is considerable variability among samples, especially with human islets, and 3–5-fold differences are not uncommon (Kayton *et al.*, 2015). Nevertheless, this observation agrees with previous studies that suggested that murine islets contain more β-cells than human islets. For example, mouse islets were found to contain a higher proportion of insulin-containing cells (77% versus 55%, $p < 0.05$) and a lower proportion of glucagon-containing

cells (18% versus 38%, $p < 0.05$) than human islets (Cabrera *et al.*, 2006). Similar proportions (averages of ~85% vs. ~60%) were also found in a study that indicated declines in β-cell content in larger human islets (Kilimnik *et al.*, 2012). Lower insulin release from human islets as compared with murine ones has been observed by others as well. For example, Dai and co-workers measured a lower first-phase peak for human versus murine islets, ~ 30 vs. 80 pg/min/IEQ, respectively, when stimulated with 16.7 mM glucose (G16.7) (Dai *et al.*, 2012); however, they also reported a higher insulin output in human islets than in mouse exposed to basal 5.6 mM glucose (G5.6). Here, at 3 mM basal glucose (G3), a clear difference between the baseline insulin secretion of human and mouse islets was not observed, but the baseline secretion varied considerably among preparations. A sharper first-phase peak and a more elevated second-phase plateau in murine islets was also observed by Henquin and co-workers in work that also found the average insulin content of mouse islets to be considerably higher than that of human islets; e.g., (Henquin *et al.*, 2006b) vs. (Henquin *et al.*, 2006a; Henquin *et al.*, 2015).

Effect of increasing capsule size

Results here reaffirm that increasing capsule size imparts an increasingly delayed and blunted first-phase response. Notably, the same effect was present not only during glucose stimulation, but also during KCl depolarization (Figure 3), indicating common diffusion limitations in both the inflow of the secretagogue and the outflow of the secreted insulin. Such delayed and blunted responses due to the impact of the encapsulating hydrogel have been found by others as well (Lim *et al.*, 1980; Chicheportiche *et al.*, 1988; Jesser *et al.*, 1996; de Vos *et al.*, 2003). Consequently, larger capsules unavoidably lead to the dampening of the insulin response and to sustained-release type insulin secretion that can only slowly respond to changes in glucose concentrations. While the delay and blunting may not always be physiologically significant, it still should be an important consideration in the design of improved bioartificial pancreas devices (Korsgren, 2017), particularly because (1) an accelerated loss of the first-phase insulin response has been found in those progressing toward T1D in several studies (Chase *et al.*, 2001; Sosenko *et al.*, 2013; Koskinen *et al.*, 2016; Veijola *et al.*, 2016) and (2) there is evidence that even if a first phase may not exist under physiological conditions following oral administration, the ability of β-cells to generate a rapidly increasing insulin profile is still relevant and particularly effective in restraining hepatic glucose production (Caumo *et al.*, 2004). Hence, lack of an adequate first-phase response might have long-term physiological consequences.

It should also be noted that the perifusion experiments reported herein were performed at atmospheric oxygen (~20% O_2; $p_{O_2} \approx 150$ mmHg; $c_{oxy} = 0.22$ mM). Similar experiments are sometimes performed with oxygen-enriched perifusion media (e.g., 95% O_2) to minimize the effects of oxygen limitation (e.g., (Jesser *et al.*, 1996; Garfinkel *et al.*, 1998; de Vos *et al.*, 2003; Henquin *et al.*, 2006a; Barrientos *et al.*, 2009)). More importantly, at lower oxygen concentrations, such as those mimicking the tissue oxygen concentrations that transplanted islets typically encounter (e.g., $p_{O_2} = 35–45$ mmHg; $c_{oxy} = 0.05–0.065$ mM), the loss in insulin secreting ability is likely to be even more significant due to the more severe hypoxia especially in the core regions of larger islets (Buchwald, 2011). For example, the present model predicts that *(i)* under low oxygen conditions free islets still secrete insulin

at 70–75% of their normal rate, but encapsulated islets decline to 50%; and *(ii)* the larger the glucose concentration, the more hampered the response (Buchwald, 2011). Various approaches have been explored to overcome this nutrient diffusion problem (Colton, 2014; Scharp *et al.*, 2014), such as the use of smaller (Halle *et al.*, 1994; Hall *et al.*, 2010; Gattás-Asfura *et al.*, 2013; Tomei *et al.*, 2014) or more oxygen-permeable capsules (Chin *et al.*, 2008; Gattás-Asfura *et al.*, 2012), the use of smaller islets/pseudoislets (O'Sullivan *et al.*, 2010; Hilderink *et al.*, 2015), the co-encapsulation of anti-inflammatory drugs (to limit fibrotic overgrowth) (Dang *et al.*, 2013), the use of islet cells that are more hypoxia-resistant (Wright *et al.*, 1998) or are engineered to contain an intracellular oxygen carrier such as myoglobin (Tilakaratne *et al.*, 2002), preimplantation (Sörenby *et al.*, 2008), and the stimulation of blood vessel growth around the implanted devices (Josephs *et al.*, 1999; Lembert *et al.*, 2005). Others focused on local oxygen delivery near the islets, for example, by *in situ* oxygen generation via an electrochemical process (Wu *et al.*, 1999), local photosynthesis (Bloch *et al.*, 2006), hydrolytically activated oxygen-generating biomaterials (Pedraza *et al.*, 2012; Coronel *et al.*, 2017), or by daily delivery into a dedicated gas chamber integrated into the transplanted device (Ludwig *et al.*, 2012; Ludwig *et al.*, 2013). Macrodevices intended to encapsulate larger tissue amounts within a single immune-isolated volume, such as TheraCyte (Geller *et al.*, 1997; Loudovaris *et al.*, 1999; O'Sullivan *et al.*, 2011) or its Encaptra modification are facing the same oxygen diffusion limitation problem, and, most likely, in an even more challenging form.

Fibrotic overgrowth can further exacerbate the problem of diffusion limitation for nutrient (mostly oxygen) availability, and the efficacy of implanted biomedical devices in general is often compromised by host recognition and subsequent foreign body responses. Depending on the nature of biomaterial as well as that of the graft (allo- vs. xeno-), overgrowth may be limited to a relatively small percent of microencapsulated islets; nevertheless, central necrosis, as well as macrophage-released factors, have still been found to limit long-term graft function (de Vos *et al.*, 1999; de Vos *et al.*, 2004). A more recent investigation suggested that the biocompatibility of (alginate) encapsulated islets is geometry dependent, and can be significantly improved by use of larger capsules, as larger spheres (i.e., $d = 1.5$ mm) generated less foreign body reaction and fibrosis than smaller spheres (Veiseh *et al.*, 2015). A notable caveat of this approach, however, is the significant increase in diffusional length it imparts. Hence, biocompatibility and diffusion limitation aspects might have to be balanced against each other.

Computational model

Quantitative models of islet function are not only of general interest to characterize the glucose–insulin regulatory system, but are of direct relevance for the design of optimal biohybrid devices. Our general, FEM-based model used here is considerably more complex than any other computational model explored to date for encapsulated islets (Pillarella *et al.*, 1990; Reach *et al.*, 1990; Todisco *et al.*, 1995; Tziampazis *et al.*, 1995; Buladi *et al.*, 1996; Dulong *et al.*, 2002; Dulong *et al.*, 2005) as those do not allow the coupling of both convective and diffusive transport with reactive rates for arbitrary geometries. Most of these models allow transport by diffusion only with only a select number that incorporate convective transport (i.e., fluid dynamics to model flow) (Pillarella *et al.*, 1990; Buladi *et al.*,

1996), and even these are restricted by cylindrical symmetry assumptions. Contrary to these, the present model can be used for arbitrary geometries and flowing fluids to calculate insulin output in response to arbitrary incoming glucose profiles (Buchwald, 2011). It can predict both first- and second-phase insulin responses, and it also incorporates an oxygen-dependence for insulin release (Figure 2). This is important because in avascular islets, the hypoxia resulting from oxygen diffusion limitations is a major limiting factor (Ohta *et al.*, 1990; Dionne *et al.*, 1993; Papas *et al.*, 1999; Sweet *et al.*, 2002; Wang *et al.*, 2005; Buchwald, 2009). Figure 8 highlights this by illustrating the calculated oxygen and glucose concentrations during high glucose (G11) exposure. The drop in oxygen is more significant than the drop in glucose, and most of the decline occurs inside of the islet. Hence, oxygen availability is the main factor limiting viability and functionality, and it is particularly severe in the core of larger islets and capsules.

In general, our calculations are in strong overall agreement, even on a quantitative level, with various experimental observations indicating that when isolated islets are maintained under normoxic conditions, larger islets show central necrosis and this becomes much more severe under hypoxic conditions (Vasir *et al.*, 1998; Giuliani *et al.*, 2005; MacGregor *et al.*, 2006; Komatsu *et al.*, 2016). This is a main reason why islet cultures require very low culture densities to ensure viability in the core of the larger islets: Current standard practice is 100–200 IEQ/cm^2 corresponding to a surface utilization of only 2–3% (Sander *et al.*, 1996; Murdoch *et al.*, 2004; Papas *et al.*, 2005; Ichii *et al.*, 2007). For the same reason, insulin production rates are more severely limited inside larger islets, as well as in larger capsules (Skiles *et al.*, 2011). This is well illustrated by the color-coding shown in Figure 7. It has to be noted that these predictions should be treated with caution as data available to calibrate the oxygen limitation of insulin secretion was limited. The present model was built using the only data published so far (Dionne *et al.*, 1993). Lacking corresponding experimental data, the effects of different diffusion coefficients within the hydrogel (e.g., due to different alginate concentrations or to incorporation of modifiers) were not modeled; however, exploratory calculations indicate that the impact should be relatively modest.

With the present recalibrations, the fit of the experimental data was not just qualitative, but also quantitative, meaning that, in addition to the overall time-profiles being similar, the calculated insulin amounts were also in good agreement with the measured ones. Note that because islets are spheroid-like cell aggregates of different sizes (<50 to 500 μm) resulting in possible thousand-fold differences between the mass contribution of individual particles, evaluation of islet mass (IEQ) is challenging and error-prone (Buchwald *et al.*, 2016), and it is especially so for encapsulated islets. Therefore, IEQ estimates are uncertain and can vary from lab to lab and from person to person. We and others have previously shown that, for the manual count of islet mass (IEQ), coefficients of variability (CV) can be as high as 30% (Buchwald *et al.*, 2009; Kissler *et al.*, 2010; Friberg *et al.*, 2011; Buchwald *et al.*, 2016). Hence, even with accurate insulin assays, up to two-fold differences in the present insulin release rate per IEQ estimates are feasible depending on laboratory practices and inter-technician variabilities. Nevertheless, the model can provide quantitative estimates, and these can serve as first estimates for future bioengineering or tissue engineering approaches.

Conclusions

In conclusion, dynamic GSIR perifusion experiments can provide a robust quantitative characterization of the insulin release kinetics of encapsulated islets. Here, we found that *(i)* human islets secrete less insulin per IEQ than murine islets and with a less pronounced first phase peak, *(ii)* small microcapsules cause only a slightly delayed and blunted first-phase insulin response compared to free islets, *(iii)* larger capsules completely blunt the first-phase peak and decrease the amount of insulin output in response to a glucose challenge, and *(iv)* our complex computational insulin secretion model gives adequate qualitative and quantitative description of the insulin secretion profile of free and hydrogel-encapsulated islets. Bioartificial pancreas type devices can provide physiologically desirable insulin release and long-term clinical solutions only if immunoisolation and biocompatibility considerations are also integrated by design with optimized nutrient diffusion and insulin release characteristics.

Acknowledgments

Financial support

Parts of this work were supported by grants from the National Institutes of Health (NIH) National Institute of Diabetes and Digestive and Kidney Diseases (NIDDK) (1UC4DK104208), the Juvenile Diabetes Research Foundation (17-2012-361, 3SRA 2017-347MB), and the Diabetes Research Institute Foundation (www.diabetesresearch.org).

Abbreviations

FEM	finite element method
GSIR	glucose-stimulated insulin release
IEQ	islet equivalent
SSE	sum of squared errors
T1D	type 1 diabetes mellitus

References

Barrientos R, Baltrusch S, Sigrist S, Legeay G, Belcourt A, Lenzen S. Kinetics of insulin secretion from MIN6 pseudoislets after encapsulation in a prototype device of a bioartificial pancreas. Horm Metab Res. 2009; 41(1):5–9. [PubMed: 18855306]

Bloch K, Papismedov E, Yavriyants K, Vorobeychik M, Beer S, Vardi P. Photosynthetic oxygen generator for bioartificial pancreas. Tissue Eng. 2006; 12(2):337–344. [PubMed: 16548692]

Bocca N, Pileggi A, Molano RD, Marzorati S, Wu W, Bodor N, et al. Soft corticosteroids for local immunosuppression: exploring the possibility for the use of loteprednol etabonate in islet transplantation. Pharmazie. 2008; 63(3):226–232. [PubMed: 18444512]

Buchwald P. FEM-based oxygen consumption and cell viability models for avascular pancreatic islets. Theor Biol Med Model. 2009; 6:art 5.

Buchwald P. A local glucose-and oxygen concentration-based insulin secretion model for pancreatic islets. Theor Biol Med Model. 2011; 8:20. [PubMed: 21693022]

Buchwald P, Bernal A, Echeverri F, Tamayo-Garcia A, Linetsky E, Ricordi C. Fully automated islet cell counter (ICC) for the assessment of islet mass, purity, and size distribution by digital image analysis. Cell Transplant. 2016; 25(10):1747–1761. [PubMed: 27196960]

Buchwald P, Cechin SR. Glucose-stimulated insulin secretion in isolated pancreatic islets: Multiphysics FEM model calculations compared to results of perifusion experiments with human islets. J Biomed Sci Eng. 2013; 6(5A):26–35.

Buchwald P, Cechin SR, Weaver JD, Stabler CL. Experimental evaluation and computational modeling of the effects of encapsulation on the time-profile of glucose-stimulated insulin release of pancreatic islets. Biomed Eng Online. 2015; 14:28. [PubMed: 25889474]

Buchwald P, Wang X, Khan A, Bernal A, Fraker C, Inverardi L, et al. Quantitative assessment of islet cell products: estimating the accuracy of the existing protocol and accounting for islet size distribution. Cell Transplant. 2009; 18(10–11):1223–1235. [PubMed: 19818209]

Buladi BM, Chang CC, Belovich JM, Gatica JE. Transport phenomena and kinetics in an extravascular bioartificial pancreas. AIChE J. 1996; 42(9):2668–2682.

Cabrera O, Berman DM, Kenyon NS, Ricordi C, Berggren PO, Caicedo A. The unique cytoarchitecture of human pancreatic islets has implications for islet cell function. Proc Natl Acad Sci USA. 2006; 103(7):2334–2339. [PubMed: 16461897]

Cabrera O, Jacques-Silva MC, Berman DM, Fachado A, Echeverri F, Poo RE, et al. Automated, high-throughput assays for evaluation of human pancreatic islet function. Cell Transplant. 2008; 16(10): 1039–1048. [PubMed: 18351020]

Calafiore R, Basta G. Clinical application of microencapsulated islets: actual prospectives on progress and challenges. Adv Drug Deliv Rev. 2014; 67–68:84–92.

Caumo A, Luzi L. First-phase insulin secretion: does it exist in real life? Considerations on shape and function. Am J Physiol Endocrinol Metab. 2004; 287(3):E371–E385. [PubMed: 15308473]

Chase HP, Cuthbertson DD, Dolan LM, Kaufman F, Krischer JP, Schatz DA, et al. First-phase insulin release during the intravenous glucose tolerance test as a risk factor for type 1 diabetes. J Pediatr. 2001; 138(2):244–249. [PubMed: 11174623]

Chicheportiche D, Reach G. In vitro kinetics of insulin release by microencapsulated rat islets: effect of the size of the microcapsules. Diabetologia. 1988; 31(1):54–57. [PubMed: 3280370]

Chin K, Khattak SF, Bhatia SR, Roberts SC. Hydrogel-perfluorocarbon composite scaffold promotes oxygen transport to immobilized cells. Biotechnol Prog. 2008; 24(2):358–366. [PubMed: 18293995]

Colton CK. Oxygen supply to encapsulated therapeutic cells. Adv Drug Deliv Rev. 2014; 67–68C:93–110.

Coronel MM, Geusz R, Stabler CL. Mitigating hypoxic stress on pancreatic islets via in situ oxygen generating biomaterial. Biomaterials. 2017; 129:139–151. [PubMed: 28342320]

Dai C, Brissova M, Hang Y, Thompson C, Poffenberger G, Shostak A, et al. Islet-enriched gene expression and glucose-induced insulin secretion in human and mouse islets. Diabetologia. 2012; 55(3):707–718. [PubMed: 22167125]

Dang TT, Thai AV, Cohen J, Slosberg JE, Siniakowicz K, Doloff JC, et al. Enhanced function of immuno-isolated islets in diabetes therapy by co-encapsulation with an anti-inflammatory drug. Biomaterials. 2013; 34(23):5792–5801. [PubMed: 23660251]

de Vos P, de Haan BJ, de Haan A, van Zanten J, Faas MM. Factors influencing functional survival of microencapsulated islet grafts. Cell Transplant. 2004; 13(5):515–524. [PubMed: 15565864]

de Vos P, Smedema I, van Goor H, Moes H, van Zanten J, Netters S, et al. Association between macrophage activation and function of micro-encapsulated rat islets. Diabetologia. 2003; 46(5): 666–673. [PubMed: 12750768]

de Vos P, van Straaten JF, Nieuwenhuizen AG, de Groot M, Ploeg RJ, de Haan BJ, et al. Why do microencapsulated islet grafts fail in the absence of fibrotic overgrowth? Diabetes. 1999; 48(7): 1381–1388. [PubMed: 10389842]

Desai T, Shea LD. Advances in islet encapsulation technologies. Nat Rev Drug Discov. 2016; 16(5): 338–350. [PubMed: 28008169]

Dionne KE, Colton CK, Yarmush ML. Effect of hypoxia on insulin secretion by isolated rat and canine islets of Langerhans. Diabetes. 1993; 42(1):12–21. [PubMed: 8420809]

Dulong JL, Legallais C. Contributions of a finite element model for the geometric optimization of an implantable bioartificial pancreas. Artif Organs. 2002; 26(7):583–589. [PubMed: 12081516]

Dulong JL, Legallais C. What are the relevant parameters for the geometrical optimization of an implantable bioartificial pancreas? J Biomech Eng. 2005; 127(7):1054–1061. [PubMed: 16502647]

Fiorina P, Shapiro AM, Ricordi C, Secchi A. The clinical impact of islet transplantation. Am J Transplant. 2008; 8(10):1990–1997. [PubMed: 18828765]

Fournier, RL. Basic Transport Phenomena in Biomedical Engineering. 3. Boca Raton, FL: CRC Press; 2011.

Friberg AS, Brandhorst H, Buchwald P, Goto M, Ricordi C, Brandhorst D, et al. Quantification of the islet product: presentation of a standardized current Good Manufacturing Practices compliant system with minimal variability. Transplantation. 2011; 91(6):677–683. [PubMed: 21248660]

Garcia-Contreras M, Tamayo-Garcia A, Pappan KL, Michelotti GA, Stabler CL, Ricordi C, et al. A metabolomics study of the effects of inflammation, hypoxia, and high glucose on isolated human pancreatic islets. J Proteome Res. 2017; 16(6):2294–2306. [PubMed: 28452488]

Garfinkel MR, Harland RC, Opara EC. Optimization of the microencapsulated islet for transplantation. J Surg Res. 1998; 76(1):7–10. [PubMed: 9695730]

Gattás-Asfura KM, Fraker CA, Stabler CL. Perfluorinated alginate for cellular encapsulation. J Biomed Mater Res A. 2012; 100(8):1963–1971. [PubMed: 22544596]

Gattás-Asfura KM, Stabler CL. Bioorthogonal layer-by-layer encapsulation of pancreatic islets via hyperbranched polymers. ACS Appl Mater Interfaces. 2013; 5(20):9964–9974. [PubMed: 24063764]

Geller RL, Loudovaris T, Neuenfeldt S, Johnson RC, Brauker JH. Use of an immunoisolation device for cell transplantation and tumor immunotherapy. Ann NY Acad Sci. 1997; 831:438–451. [PubMed: 9616733]

Giuliani M, Moritz W, Bodmer E, Dindo D, Kugelmeier P, Lehmann R, et al. Central necrosis in isolated hypoxic human pancreatic islets: evidence for postisolation ischemia. Cell Transplant. 2005; 14(1):67–76. [PubMed: 15789664]

Gregg EW, Li Y, Wang J, Burrows NR, Ali MK, Rolka D, et al. Changes in diabetes-related complications in the United States, 1990–2010. N Engl J Med. 2014; 370(16):1514–1523. [PubMed: 24738668]

Hall KK, Gattas-Asfura KM, Stabler CL. Microencapsulation of islets within alginate/poly(ethylene glycol) gels cross-linked via Staudinger ligation. Acta Biomater. 2010; 7(2):614–624. [PubMed: 20654745]

Halle JP, Leblond FA, Pariseau JF, Jutras P, Brabant MJ, Lepage Y. Studies on small (< 300 microns) microcapsules: II--Parameters governing the production of alginate beads by high voltage electrostatic pulses. Cell Transplant. 1994; 3(5):365–372. [PubMed: 7827774]

Hedeskov CJ. Mechanism of glucose-induced insulin secretion. Physiol Rev. 1980; 60(2):442–509. [PubMed: 6247727]

Henquin JC. Triggering and amplifying pathways of regulation of insulin secretion by glucose. Diabetes. 2000; 49(11):1751–1760. [PubMed: 11078440]

Henquin JC. Regulation of insulin secretion: a matter of phase control and amplitude modulation. Diabetologia. 2009; 52(5):739–751. [PubMed: 19288076]

Henquin JC, Dufrane D, Kerr-Conte J, Nenquin M. Dynamics of glucose-induced insulin secretion in normal human islets. Am J Physiol Endocrinol Metab. 2015; 309(7):E640–E650. [PubMed: 26264556]

Henquin JC, Dufrane D, Nenquin M. Nutrient control of insulin secretion in isolated normal human islets. Diabetes. 2006a; 55(12):3470–3477. [PubMed: 17130494]

Henquin JC, Nenquin M, Stiernet P, Ahren B. In vivo and in vitro glucose-induced biphasic insulin secretion in the mouse: pattern and role of cytoplasmic Ca2+ and amplification signals in beta-cells. Diabetes. 2006b; 55(2):441–451. [PubMed: 16443779]

Hering BJ, Clarke WR, Bridges ND, Eggerman TL, Alejandro R, Bellin MD, et al. Phase 3 trial of transplantation of human islets in type 1 diabetes complicated by severe hypoglycemia. Diabetes Care. 2016; 39(7):1230–1240. [PubMed: 27208344]

Hilderink J, Spijker S, Carlotti F, Lange L, Engelse M, van Blitterswijk C, et al. Controlled aggregation of primary human pancreatic islet cells leads to glucose-responsive pseudoislets comparable to native islets. J Cell Mol Med. 2015; 19(8):1836–1846. [PubMed: 25782016]

Ichii, H., Pileggi, A., Khan, A., Fraker, C., Ricordi, C. Culture and transportation of human islets between centers. In: Shapiro, AMJ., Shaw, JAM., editors. Islet Transplantation and Beta Cell Replacement Therapy. New York: Informa Healthcare; 2007. p. 251-268.

Jesser C, Kessler L, Lambert A, Belcourt A, Pinget M. Pancreatic islet macroencapsulation: a new device for the evaluation of artificial membrane. Artif Organs. 1996; 20(9):997–1007. [PubMed: 8864021]

Johnson JD. The quest to make fully functional human pancreatic beta cells from embryonic stem cells: climbing a mountain in the clouds. Diabetologia. 2016; 59(10):2047–2057. [PubMed: 27473069]

Josephs SF, Loudovaris T, Dixit A, Young SK, Johnson RC. In vivo delivery of recombinant human growth hormone from genetically engineered human fibroblasts implanted within Baxter immunoisolation devices. J Mol Med. 1999; 77(1):211–214. [PubMed: 9930965]

Kayton NS, Poffenberger G, Henske J, Dai C, Thompson C, Aramandla R, et al. Human islet preparations distributed for research exhibit a variety of insulin-secretory profiles. Am J Physiol Endocrinol Metab. 2015; 308(7):E592–E602. [PubMed: 25648831]

Khan, A., Pileggi, A., Ricordi, C. Islet cell products: processing, quality controls and implications for bioartificial applications. In: Hallé, JP.de Vos, P., Rosenberg, L., editors. The Bioartificial Pancreas and other Biohybrid Therapies. Trivandrum, India: Research Signpost; 2009. p. 383-402.

Kilimnik G, Jo J, Periwal V, Zielinski MC, Hara M. Quantification of islet size and architecture. Islets. 2012; 4(2):167–172. [PubMed: 22653677]

King S. The evolution of islet encapsulation ventures. History of diabetes research. 2009; 2010

Kissler HJ, Niland JC, Olack B, Ricordi C, Hering BJ, Naji A, et al. Validation of methodologies for quantifying isolated human islets: an islet cell resources study. Clin Transplant. 2010; 24(2):236–242. [PubMed: 19719726]

Komatsu H, Kang D, Medrano L, Barriga A, Mendez D, Rawson J, et al. Isolated human islets require hyperoxia to maintain islet mass, metabolism, and function. Biochem Biophys Res Commun. 2016; 470(3):534–538. [PubMed: 26801563]

Korsgren O. Islet encapsulation: physiological possibilities and limitations. Diabetes. 2017; 66(7): 1748–1754. [PubMed: 28637827]

Koskinen MK, Helminen O, Matomaki J, Aspholm S, Mykkanen J, Makinen M, et al. Reduced beta-cell function in early preclinical type 1 diabetes. Eur J Endocrinol. 2016; 174(3):251–259. [PubMed: 26620391]

Lacy PE, Walker MM, Fink CJ. Perifusion of isolated rat islets in vitro. Participation of the microtubular system in the biphasic release of insulin. Diabetes. 1972; 21(10):987–998. [PubMed: 4561331]

Lembert N, Wesche J, Petersen P, Doser M, Zschocke P, Becker HD, et al. Encapsulation of islets in rough surface, hydroxymethylated polysulfone capillaries stimulates VEGF release and promotes vascularization after transplantation. Cell Transplant. 2005; 14(2–3):97–108.

Lim F, Sun AM. Microencapsulated islets as bioartificial endocrine pancreas. Science. 1980; 210(4472):908–910. [PubMed: 6776628]

Loudovaris T, Jacobs S, Young S, Maryanov D, Brauker J, Johnson RC. Correction of diabetic nod mice with insulinomas implanted within Baxter immunoisolation devices. J Mol Med. 1999; 77(1): 219–222. [PubMed: 9930967]

Ludwig B, Reichel A, Steffen A, Zimerman B, Schally AV, Block NL, et al. Transplantation of human islets without immunosuppression. Proc Natl Acad Sci USA. 2013; 110(47):19054–19058. [PubMed: 24167261]

Ludwig B, Rotem A, Schmid J, Weir GC, Colton CK, Brendel MD, et al. Improvement of islet function in a bioartificial pancreas by enhanced oxygen supply and growth hormone releasing hormone agonist. Proc Natl Acad Sci USA. 2012 ePub.

MacGregor RR, Williams SJ, Tong PY, Kover K, Moore WV, Stehno-Bittel L. Small rat islets are superior to large islets in in vitro function and in transplantation outcomes. Am J Physiol Endocrinol Metab. 2006; 290(5):E771–E779. [PubMed: 16303846]

Mahla RS. Stem cells: applications in regenerative medicine and disease therapeutics. Int J Cell Biol. 2016; 2016:6940283. [PubMed: 27516776]

Murdoch TB, McGhee-Wilson D, Shapiro AM, Lakey JR. Methods of human islet culture for transplantation. Cell Transplant. 2004; 13(6):605–617.

O'Sullivan ES, Johnson AS, Omer A, Hollister-Lock J, Bonner-Weir S, Colton CK, et al. Rat islet cell aggregates are superior to islets for transplantation in microcapsules. Diabetologia. 2010; 53(5): 937–945. [PubMed: 20101386]

O'Sullivan ES, Vegas A, Anderson DG, Weir GC. Islets transplanted in immunoisolation devices: a review of the progress and the challenges that remain. Endocr Rev. 2011; 32(6):827–844. [PubMed: 21951347]

Ohta M, Nelson D, Nelson J, Meglasson MD, Erecinska M. Oxygen and temperature dependence of stimulated insulin secretion in isolated rat islets of Langerhans. J Biol Chem. 1990; 265(29): 17525–17532. [PubMed: 2211646]

Pambianco G, Costacou T, Ellis D, Becker DJ, Klein R, Orchard TJ. The 30-year natural history of type 1 diabetes complications: the Pittsburgh Epidemiology of Diabetes Complications Study experience. Diabetes. 2006; 55(5):1463–1469. [PubMed: 16644706]

Papas KK, Avgoustiniatos ES, Tempelman LA, Weir GC, Colton CK, Pisania A, et al. High-density culture of human islets on top of silicone rubber membranes. Transplant Proc. 2005; 37(8):3412–3414. [PubMed: 16298611]

Papas KK, Long RC Jr, Sambanis A, Constantinidis I. Development of a bioartificial pancreas: II. Effects of oxygen on long-term entrapped betaTC3 cell cultures. Biotechnol Bioeng. 1999; 66(4): 231–237. [PubMed: 10578093]

Pedraza E, Coronel MM, Fraker CA, Ricordi C, Stabler CL. Preventing hypoxia-induced cell death in beta cells and islets via hydrolytically activated, oxygen-generating biomaterials. Proc Natl Acad Sci USA. 2012

Pileggi A, Molano RD, Berney T, Cattan P, Vizzardelli C, Oliver R, et al. Heme oxygenase-1 induction in islet cells results in protection from apoptosis and improved in vivo function after transplantation. Diabetes. 2001; 50(9):1983–1991. [PubMed: 11522663]

Pillarella MR, Zydney AL. Theoretical analysis of the effect of convective flow on solute transport and insulin release in a hollow fiber bioartificial pancreas. J Biomech Eng. 1990; 112(2):220–228. [PubMed: 2189042]

Reach G, Jaffrin MY. Kinetic modelling as a tool for the design of a vascular bioartificial pancreas: feedback between modelling and experimental validation. Comput Methods Programs Biomed. 1990; 32(3–4):277–285. [PubMed: 2249427]

Rengifo HR, Giraldo JA, Labrada I, Stabler CL. Long-term survival of allograft murine islets coated via covalently stabilized polymers. Adv Healthc Mater. 2014; 3(7):1061–1070. [PubMed: 24497465]

Ricordi C, Goldstein JS, Balamurugan AN, Szot GL, Kin T, Liu C, et al. National Institutes of Health-Sponsored Clinical Islet Transplantation Consortium Phase 3 Trial: Manufacture of a complex cellular product at eight processing facilities. Diabetes. 2016; 65(11):3418–3428. [PubMed: 27465220]

Ricordi C, Gray DWR, Hering BJ, Kaufman DB, Warnock GL, Kneteman NM, et al. Islet isolation assessment in man and large animals. Acta Diabetol Lat. 1990; 27(3):185–195. [PubMed: 2075782]

Ricordi C, Lacy PE, Finke EH, Olack BJ, Scharp DW. Automated method for isolation of human pancreatic islets. Diabetes. 1988; 37(4):413–420. [PubMed: 3288530]

Ricordi C, Strom TB. Clinical islet transplantation: advances and immunological challenges. Nat Rev Immunol. 2004; 4(4):259–268. [PubMed: 15057784]

Rorsman P, Eliasson L, Renstrom E, Gromada J, Barg S, Gopel S. The cell physiology of biphasic insulin secretion. News Physiol Sci. 2000; 15:72–77. [PubMed: 11390882]

Sander, S., Eizirik, DL. Culture of human pancreatic islet cells. In: Jones, GE., editor. Methods in Molecular Medicine - Human Cell Culture Protocols. Totowa, NJ: Humana Press Inc; 1996. p. 391-407.

Scharp DW, Marchetti P. Encapsulated islets for diabetes therapy: history, current progress, and critical issues requiring solution. Adv Drug Deliv Rev. 2014; 67–68:35–73.

Shapiro AM, Pokrywczynska M, Ricordi C. Clinical pancreatic islet transplantation. Nat Rev Endocrinol. 2017; 13(5):268–277. [PubMed: 27834384]

Silva AI, de Matos AN, Brons IG, Mateus M. An overview on the development of a bio-artificial pancreas as a treatment of insulin-dependent diabetes mellitus. Med Res Rev. 2006; 26(2):181–222. [PubMed: 16342061]

Skiles ML, Fancy R, Topiwala P, Sahai S, Blanchette JO. Correlating hypoxia with insulin secretion using a fluorescent hypoxia detection system. J Biomed Mater Res B Appl Biomater. 2011; 97B(1):148–155.

Song S, Roy S. Progress and challenges in macroencapsulation approaches for type 1 diabetes (T1D) treatment: Cells, biomaterials, and devices. Biotechnol Bioeng. 2016; 113(7):1381–1402. [PubMed: 26615050]

Soon-Shiong P. Treatment of type I diabetes using encapsulated islets. Adv Drug Deliv Rev. 1999; 35(2–3):259–270. [PubMed: 10837701]

Sörenby AK, Kumagai-Braesch M, Sharma A, Hultenby KR, Wernerson AM, Tibell AB. Preimplantation of an immunoprotective device can lower the curative dose of islets to that of free islet transplantation: studies in a rodent model. Transplantation. 2008; 86(2):364–366. [PubMed: 18645504]

Sosenko JM, Skyler JS, Beam CA, Krischer JP, Greenbaum CJ, Mahon J, et al. Acceleration of the loss of the first-phase insulin response during the progression to type 1 diabetes in diabetes prevention trial-type 1 participants. Diabetes. 2013; 62(12):4179–4183. [PubMed: 23863814]

Steele JA, Halle JP, Poncelet D, Neufeld RJ. Therapeutic cell encapsulation techniques and applications in diabetes. Adv Drug Deliv Rev. 2014; 67–68:74–83.

Sweet IR, Khalil G, Wallen AR, Steedman M, Schenkman KA, Reems JA, et al. Continuous measurement of oxygen consumption by pancreatic islets. Diabetes Technol Therap. 2002; 4(5): 661–672. [PubMed: 12450449]

Teramura Y, Iwata H. Bioartificial pancreas microencapsulation and conformal coating of islet of Langerhans. Adv Drug Deliv Rev. 2010; 62(7–8):827–840. [PubMed: 20138097]

Thabit H, Hovorka R. Coming of age: the artificial pancreas for type 1 diabetes. Diabetologia. 2016; 59(9):1795–1805. [PubMed: 27364997]

Tilakaratne HK, Hunter SK, Rodgers VG. Mathematical modeling of myoglobin facilitated transport of oxygen in devices containing myoglobin-expressing cells. Math Biosci. 2002; 176(2):253–267. [PubMed: 11916512]

Todisco S, Calabro V, Iorio G. A lumped parameter mathematical model of a hollow fiber membrane device for the controlled insulin release. J Membr Sci. 1995; 106:221–232.

Tomei AA, Manzoli V, Fraker CA, Giraldo J, Velluto D, Najjar M, et al. Device design and materials optimization of conformal coating for islets of Langerhans. Proc Natl Acad Sci USA. 2014; 111(29):10514–10519. [PubMed: 24982192]

Tziampazis E, Sambanis A. Tissue engineering of a bioartificial pancreas: modeling the cell environment and device function. Biotechnol Prog. 1995; 11(2):115–126. [PubMed: 7766095]

Vasir B, Aiello LP, Yoon KH, Quickel RR, Bonner-Weir S, Weir GC. Hypoxia induces vascular endothelial growth factor gene and protein expression in cultured rat islet cells. Diabetes. 1998; 47(12):1894–1903. [PubMed: 9836521]

Veijola R, Koskinen M, Helminen O, Hekkala A. Dysregulation of glucose metabolism in preclinical type 1 diabetes. Pediatr Diabetes. 2016; 17(Suppl 22):25–30. [PubMed: 27411433]

Veiseh O, Doloff JC, Ma M, Vegas AJ, Tam HH, Bader AR, et al. Size- and shape-dependent foreign body immune response to materials implanted in rodents and non-human primates. Nat Mater. 2015; 14(6):643–651. [PubMed: 25985456]

Wang W, Upshaw L, Strong DM, Robertson RP, Reems J. Increased oxygen consumption rates in response to high glucose detected by a novel oxygen biosensor system in non-human primate and human islets. J Endocrinol. 2005; 185(3):445–455. [PubMed: 15930171]

Wright JR Jr, Yang H, Dooley KC. Tilapia - a source of hypoxia-resistant islet cells for encapsulation. Cell Transplant. 1998; 7(3):299–307. [PubMed: 9647439]

Wu H, Avgoustiniatos ES, Swette L, Bonner-Weir S, Weir GC, Colton CK. In situ electrochemical oxygen generation with an immunoisolation device. Ann NY Acad Sci. 1999; 875:105–125. [PubMed: 10415561]

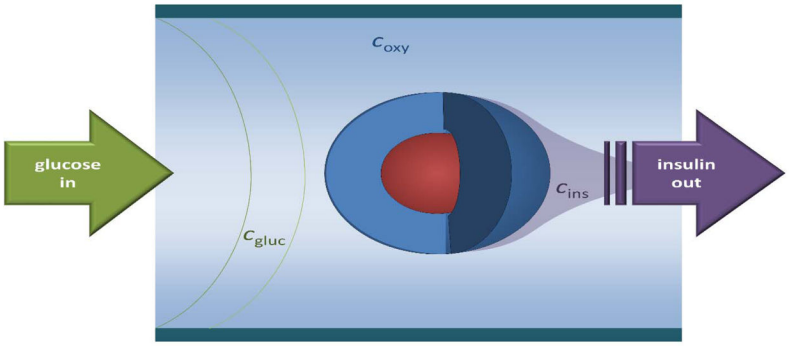

Figure 1. Schematic concept of the dynamic perifusion assay used to assess glucose-stimulated insulin release (GSIR) of free or encapsulated pancreatic islet

An idealized spherical islet (red) is shown with a hydrogel capsule (dark blue). As indicated, the perifusing solution, which has fully adjustable incoming glucose concentration, flows from left to right, and it is collected at the output to assess its insulin content.

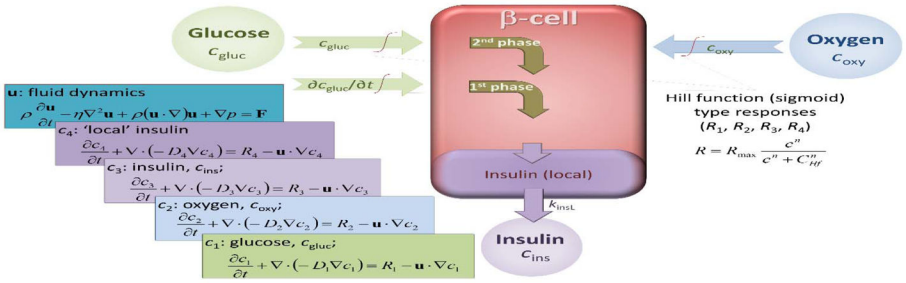

Figure 2. Conceptual representation of the present FEM computational model of insulin release

Insulin secretion is determined by the local glucose concentration, c_{gluc}, and its rate of change, $\partial c_{gluc}/\partial t$, but it is also influenced by the local oxygen concentration, c_{oxy}. The model uses a total of five coupled modules for glucose, oxygen, and insulin concentrations with incorporated fluid dynamics, as indicated by the corresponding equations on the left side.

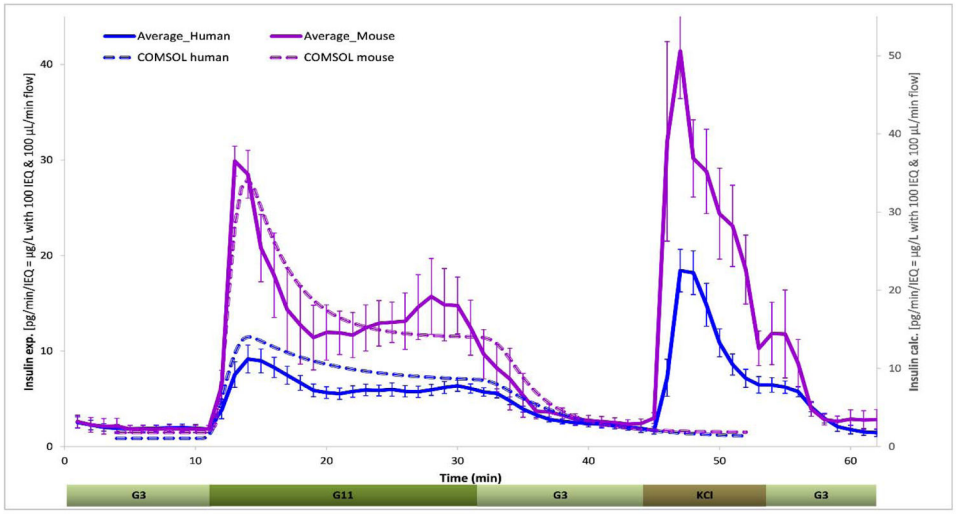

Figure 3. Dynamic GSIR in isolated human and murine islets

Summary of all experimental data collected for free murine and human islets perifused using a low (3 mM; G3, 5 min) → high (11 mM; G11, 20 min) → low (3 mM; G3, 15 min) incoming glucose stimulation (plus 10 min KCl followed by G3) as shown. Automated PERI4-02 multichannel perifusion apparatus used (samples collected every minute; 0.1 mL/min flow rate, ~100 IEQ per channel). Data are average ± SEM from multiple isolations (single or duplicate channels perifused; $n = 12$ total samples for both human and murine). Dashed lines are calculated values using the present COMSOL Multiphysics model.

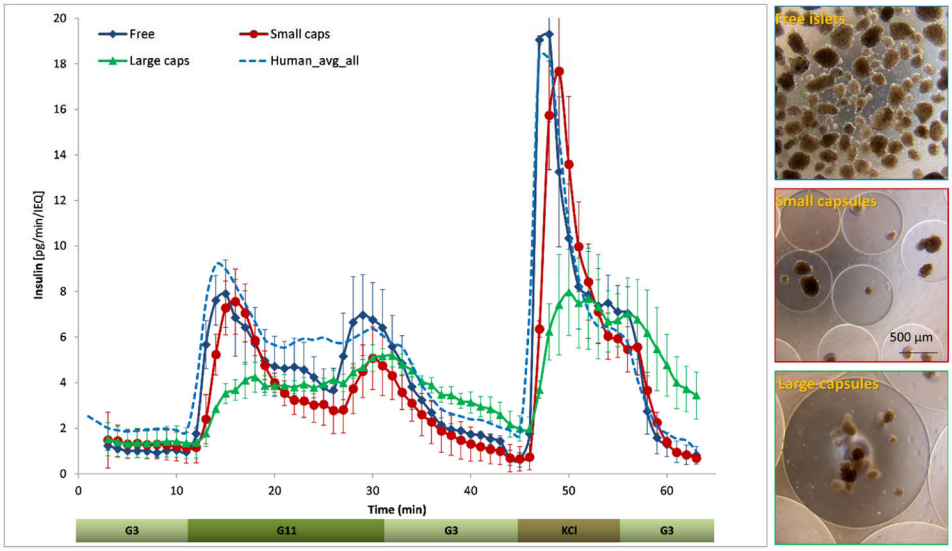

Figure 4. Glucose-induced insulin secretion in free and encapsulated human islets obtained in parallel perifusion experiments

Average of experimental data for free, as well as small and large alginate-encapsulated (d = 700 & 1800 μm) human islets perifused using the same protocol as described in Figure 3. Data are average ± SEM from multiple isolations (n = 3 for each condition sourced from the same islet preparation and conducted in parallel). The average of all free human islet perifusions shown in Figure 3 is included for reference (dashed line), and a set of illustrative phase contrast microscope images of free and encapsulated islet samples are shown at right.

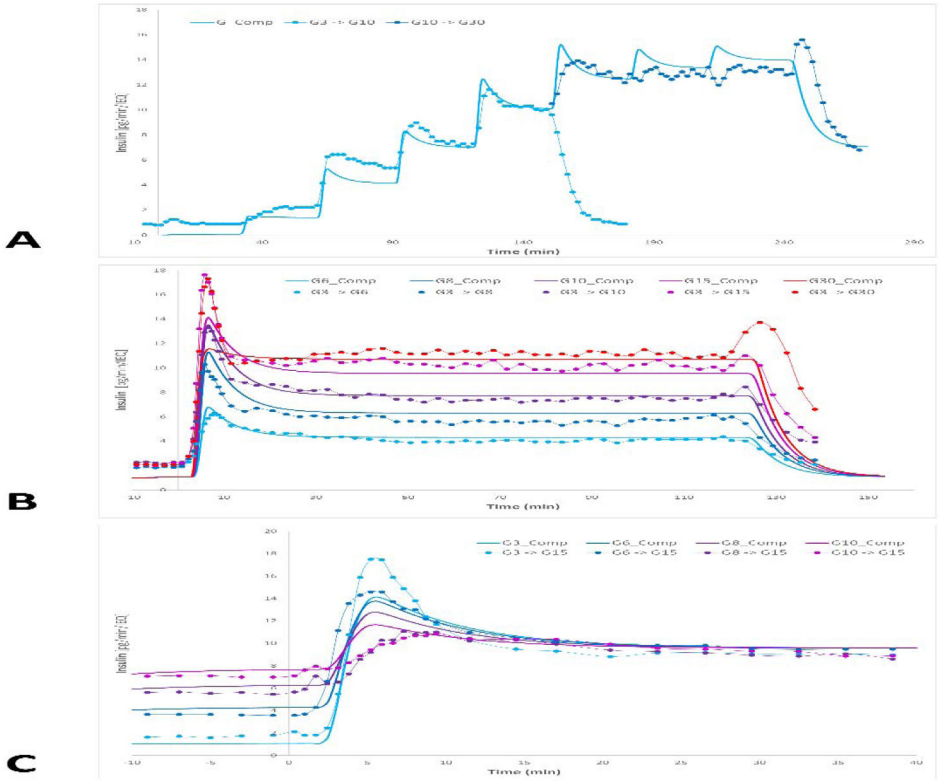

Figure 5. Additional dose-response GSIR data used for further calibration of the present computational model

Dynamic perifusion data from three different dose-response experiments from Henquin and co-workers (Henquin *et al.*, 2006a; Henquin *et al.*, 2015) used for fine-tuning the first- and second-phase insulin response calculated by the present COMSOL Multiphysics model. A variety of incoming glucose step-up challenges were used, as indicated by color-coded symbols: sequential steps of G1 → G3 → G5 → G7 → G10 and then G10 → G15 → G20 → G30 → G7 for the same preparation (**A**), different single-step challenges of G3 → G6/G8/G10/G15/G30 (**B**), and different single-step challenges of G3/G6/G8/G10 → G15 (**C**). Data (symbols) were obtained on a pg/min/IEQ scale here by using the average percent secretion values published with the average insulin content per islet from the same work (17.8 ng/islet; (Henquin *et al.*, 2015)). Continuous thicker lines of corresponding colors are values calculated with the present model.

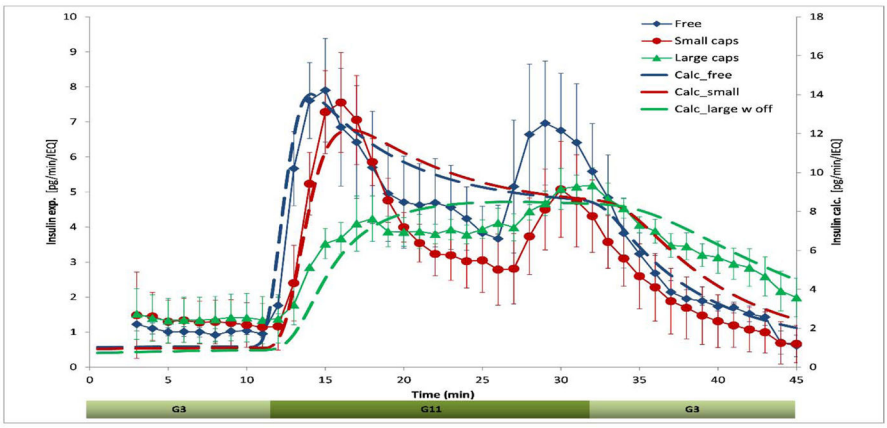

Figure 6. Fit of experimental GSIR data (free and encapsulated islets) with the present computational model

Experimental data are reproduced from Figure 4, calculated values were obtained as described in the text and converted to pg/min/IEQ for ease in comparison.

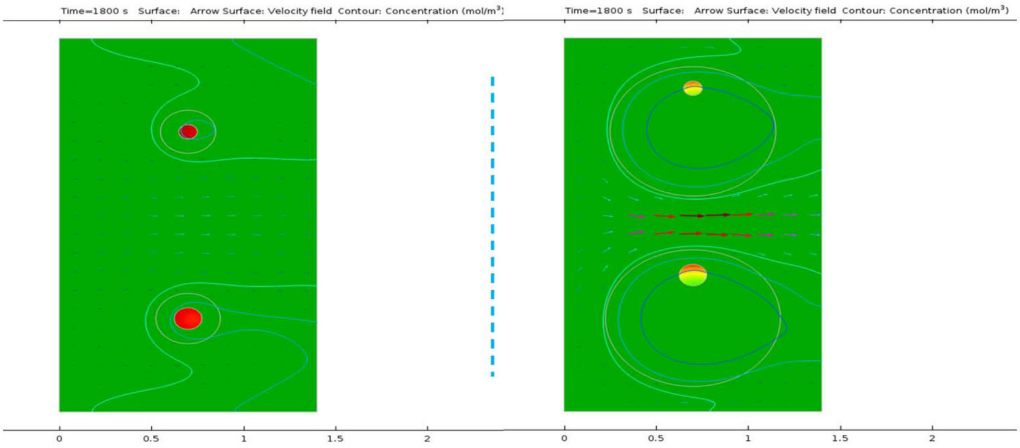

Figure 7. Model-calculated insulin production rates in response to increasing glucose concentrations

(i.e., during the first-phase response). Calculated insulin production rates for two islets (d = 100 & 150 μm – at the top and bottom, respectively) with small and large capsules (l_{caps} = 100 and 400 μm; left and right, respectively) under normoxic conditions. Data shown as surface plot are insulin production rates (color-coded from green for low to red for high). Streamlines show the flow of the perifusion fluid (color-coded for velocity; flow from left to right) and colored contour lines show isolevels for the perifusing glucose (from light blue for low to light red for high). Model calculated values are shown during the increase of the glucose concentration from 3 mM to 11 mM; first phase response is noticeably delayed and blunted in the large capsule.

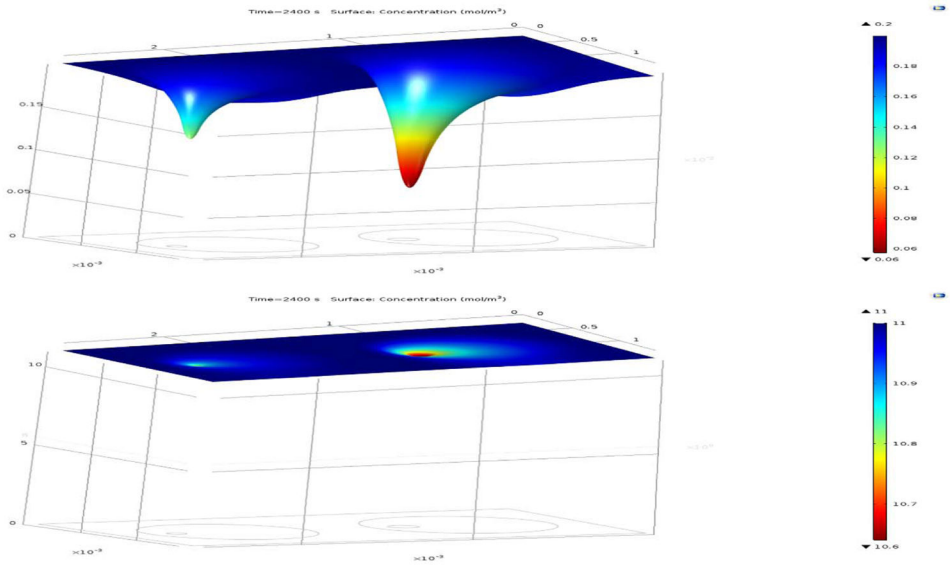

Figure 8. Diffusion limitation of oxygen versus glucose in avascular islets

Model-calculated oxygen (top) and glucose (bottom) concentrations during high glucose (G11) exposure in two encapsulated islets with d = 100 & 150 μm, l_{caps} = 400 μm (with offset) under normoxic conditions. Data shown as surface plots that are also color-coded from blue for high to red for low to illustrate that oxygen diffusion is the main limiting factor as it decreases more severely inside the islets than glucose. Data are shown at 11 mM glucose exposure under normoxic conditions (atmospheric oxygen; ~20% ≈ 0.2 mM). Oxygen limitations are even more severe for transplanted islets exposed to tissue oxygen concentrations only (~5% ≈ 0.06 mM).

Table 1

Diffusion coefficient used in the present model, $D\,[\mathrm{m}^2\cdot\mathrm{s}^{-1}]$.

Species\Media	Water	Tissue (islet)	Alginate (capsule)
Oxygen, D_{oxy}	3.0×10^{-9}	2.0×10^{-9}	2.5×10^{-9}
Glucose, D_{gluc}	0.9×10^{-9}	0.3×10^{-9}	0.6×10^{-9}
Insulin, D_{ins}	0.15×10^{-9}	0.05×10^{-9}	0.1×10^{-9}

Table 2

Summary of Hill function parameters used in the present model (Figure 1 and eq. 2; for detailed equations see (Buchwald, 2011)).

Rate	Var.	C_{Hf}	n	R_{max}	Property and comments
R_{oxy}	c_{oxy}	1 μM	1	−0.034 mol/m^3/s	Oxygen consumption, basic part. Cut to 0 below critical value, $c_{oxy} < C_{cr,oxy}$.
R_{oxy}	c_{gluc}	7 mM	2.5	N/A	Oxygen consumption, $\varphi_{o,g}$ metabolic part. Follows increase in metabolic demand; parallels second-phase insulin secretion rate.
R_{gluc}	c_{gluc}	10 μM	1	−0.028 mol/m^3/s	Glucose consumption. Under most conditions, it has no significant influence on insulin secretion.
$R_{ins,ph2}$	c_{gluc}	7 mM	2.5	H: 1.8×10^{-5} mol/m^3/s M: 3×10^{-5} mol/m^3/s	Insulin secretion rate (second-phase). Total secretion rate is modulated by local oxygen availability (last row). H and M denote values used for human and murine islets, respectively.
$R_{ins,ph1}$	c'_t ($\partial c_{gluc}/\partial t$)	0.03 mM/s	2	H: 10×10^{-5} mol/m^3/s M: 21×10^{-5} mol/m^3/s	Insulin secretion rate (first-phase). Modulated to have maximum sensibility around c_{gluc} = 5 mM and be limited at very large or low c_{gluc}. Hill slope of modulating function, $\sigma_{i1,g}$, changed to 2.5 (previously 4) for a wider range response in phase 1. Release rates k_{insL} are H: 0.003, M: 0.006 s^{-1}.
R_{ins}, $\varphi_{o,g}$	c_{oxy}	3 μM	3	N/A	Oxygen modulation of insulin secretion rate, $\varphi_{o,g}$. Limits insulin secretion if c_{oxy} becomes critically low.